Injectable and in situ foaming shape-adaptive porous Bio-based polyurethane scaffold used for cartilage regeneration

Abudureheman Bahatibieke [a,1], Shuai Wei [b,c,1], Han Feng [b,d], Jianming Zhao [a], Mengjiao Ma [a], Junfei Li [a], Yajie Xie [a], Kun Qiao [a], Yanseng Wang [a], Jiang Peng [b], Haoye Meng [b,**], Yudong Zheng [a,*]

[a] School of Materials Science and Engineering, University of Science and Technology Beijing, Beijing, 100083, China
[b] Institute of Orthopaedics, Chinese PLA General Hospital, Beijing, 100853, China
[c] Department of Orthopedics, The Second Affiliated Hospital of Soochow University, Suzhou, Jiangsu, 215004, China
[d] Hebei North University, Zhangjiakou, 075000, Hebei Province, China

ARTICLE INFO

ABSTRACT

Irregular articular cartilage injury is a common type of joint trauma, often resulting from intense impacts and other factors that lead to irregularly shaped wounds, the limited regenerative capacity of cartilage and the mismatched shape of the scaffods have contributed to unsatisfactory therapeutic outcomes. While injectable materials are a traditional solution to adapt to irregular cartilage defects, they have limitations, and injectable materials often lack the porous microstructures favorable for the rapid proliferation of cartilage cells. In this study, an injectable porous polyurethane scaffold named PU-BDO-Gelatin-Foam (PUBGF) was prepared. After injection into cartilage defects, PUBGF forms in situ at the site of the defect and exhibits a dynamic microstructure during the initial two weeks. This dynamic microstructure endows the scaffold with the ability to retain substances within its interior, thereby enhancing its capacity to promote chondrogenesis. Furthermore, the chondral repair efficacy of PUBGF was validated by directly injecting it into rat articular cartilage injury sites. The injectable PUBGF scaffold demonstrates a superior potential for promoting the repair of cartilage defects when compared to traditional porous polyurethane scaffolds. The substance retention ability of this injectable porous scaffold makes it a promising option for clinical applications.

1. Introduction

The articular cartilage serves as a crucial weight-bearing and locomotive organ within the body [1–3]. Commonly, severe impact or torsion can lead to fragmentation injuries in the knee cartilage. Such injuries typically manifest as irregular in shape, leading to an imbalance of stress in the affected region, thus causing additional harm to the cartilage [4]. Moreover, the absence of blood vessels and other specific characteristics of articular cartilage greatly limits its capacity for self-repair. Consequently, the clinical treatment of irregular articular cartilage presents a formidable challenge [5,6].

Injectable materials serve as a conducive resolution to adapt to irregular defects stemming from injury, the biomaterial can be hardened in place, in a way that completely fills the defect geometry [3]. Tissue defects of irregular profile can undergo minimally invasive remediation with these injectable substances, equilibrating stress distribution at the defective sites, an aspect of paramount relevance for the rectification of irregular cartilage defects [7–10]. Injectable materials, for instance, injectable hydrogels, have been thoroughly examined in the realm of cartilage repair. Owing to the incongruity between the medium osmotic pressure and properties intrinsic to the hydrogel [11–13], swelling is a commonplace issue in injectable hydrogels. This swelling may precipitate alterations to the mechanical performance and microscopic structure of the hydrogel [14]. Injectable hydrogels frequently demonstrate subpar mechanical attributes, proving difficult to sustain over extended periods, thus wielding a considerable impact on the reconstruction of

---

cartilage [15].

In light of the characteristics of articular cartilage, porous and elastic materials are of paramount importance for promoting cartilage regeneration [16–18]. Interconnected pores permit the dissemination of nutrients and cellular proliferation. An appropriate pore size and porosity provide favorable conditions for the adhesion and growth of chondrocytes, addressing the issue of slow cartilage cell growth [19]. However, porous scaffolds face challenges when dealing with irregular cartilage defects; conventional porous scaffolds often confront the difficulty of achieving the perfect conformation to match the shape of the wound, leading to an uneven distribution of stress at the site of the cartilage defect and resulting in degenerative cartilage diseases. The combination of injectable materials with porous scaffolds effectively resolves this problem [20,21].

Polyurethane foam are polymers formed by the reaction of isocyanates with polyols, and when pre-polyurethane is mixed with water, a polymerization reaction occurs and a large amount of carbon dioxide is released [22]. During this process, the material transitions from a liquid to a solid state, forming foamed polyurethane, which has been widely employed in the manufacturing and construction industry [23,24]. Given the characteristics of the foamed polyurethane formation process, it is theoretically well-suited for filling irregular structures. Porous polyurethane scaffolds have been studied for cartilage repair, but research on *in vivo* molding through direct injection is limited. This is mainly because the formation process involves small molecule diffusion, and after molding, the cells cannot penetrate the outermost layer of porous polyurethane due to its closed nature, impeding research on the application of injectable polyurethane in the medical materials field [25–28]. Utilizing the injectability and high porosity of foamed polyurethane to develop it into a material that can be injected *in vivo*, directly forming a porous scaffold at the site of internal defects for the repair of irregular joint cartilage damage, poses an urgent issue awaiting resolution [29].

This study introduces an injectable porous scaffold, PUBGF, which boasts remarkable shape and mechanical adaptability, coupled with a substantial material retention capability within two weeks post-injection, addressing the challenging clinical conundrum of irregular cartilage defects (Fig. 1). The scaffold's biocompatibility is enhanced by integrating gelatin and 1,4-butanediol (BDO), which also endows it with a dynamic micro-architecture. Initially, it presents with a compact porous structure, evolving slowly as the gelatin chains in the PUBGF swiftly degrade over the initial fortnight, culminating in the retention of copious gelatin degradation products within the scaffold to bolster cartilage growth. Moreover, gelatin and BDO mitigate the diffusion of small molecules. We scrutinized the physicochemical structure of the PUBGF scaffold post-injection, along with its dynamic micro-architecture, by conducting degradation experiments to assess the retention of degraded gelatin chains within the PUBGF and employing finite element analysis of fluid dynamics to simulate this feature. Cytotoxicity evaluations and chondrogenic differentiation potential were determined through cellular assays specifically designed for the injectable PUBGF scaffold. Lastly, by establishing cartilage defects in the knees of rats and directly injecting PUBGF, we comprehensively examined the metabolic toxicity of injectable PUBGF via blood biochemistry assays, gauged its impact on the subchondral bone through gait analysis and CT assessments, and evaluated the reparative effects on rat cartilage through histopathological sections.

2. Experiments and methods

2.1. Chemicals and reagents

The following reagents for the investigations and syntheses were used: polyethylene glycol (PEG, Mw = 1000, Yuanye Bio, Shanghai, China), polyoxyl Castor Oil (EL-20, Yuanye Bio, Shanghai, China), isophorone diisocyanate (IPDI, Aladdin, Shanghai, China), gelatin (Aladdin, Shanghai, China), butane-1,4-diol (BDO, Sinopharm Shanghai Test, Shanghai, China), deionized water. Except for deionized water, all
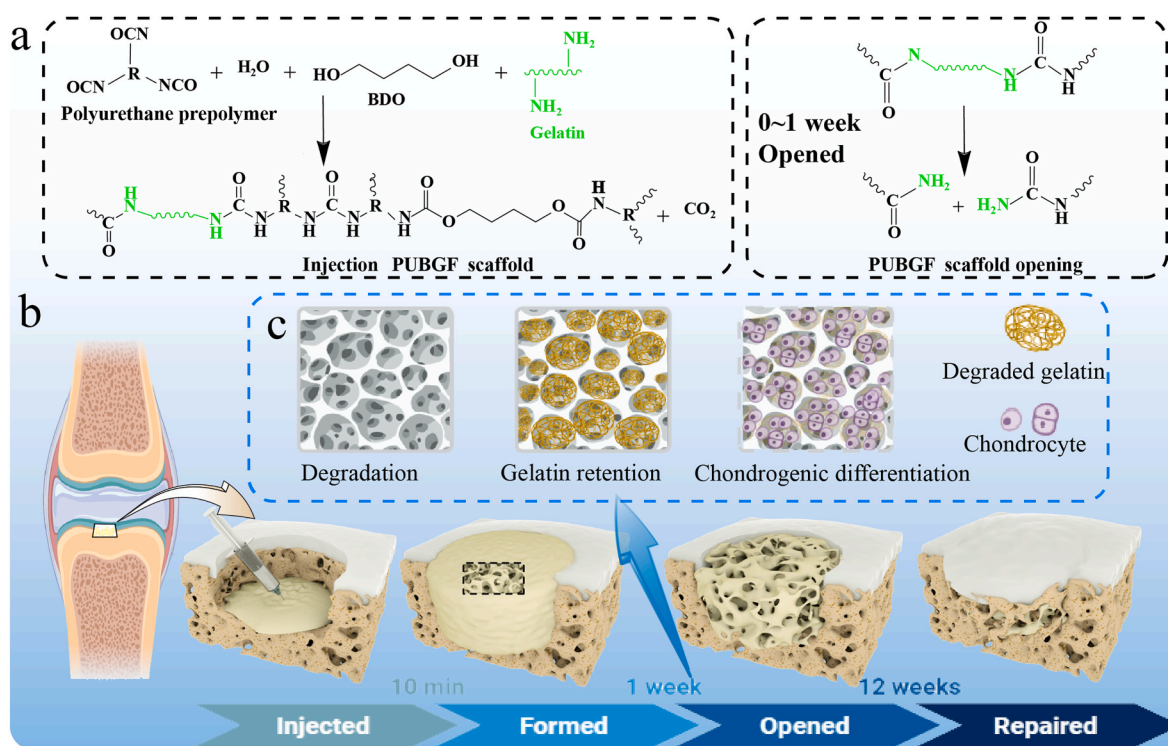

Fig. 1. (a) The mechanism of formed and opening of PUBGF after injection; (b) PUBGF scaffold injection, molding, perforation diagram and mechanism of promoting cartilage repair; (c) The injectable PUBGF scaffold exhibits dynamic microstructure and the ability to retain degradation products at 0–2 weeks, which promotes the differentiation of chondrocytes, created with BioRender.com.

chemical reagents are dried before use.

2.2. Preparation of injectable scaffold

Injectable scaffold was synthesized using a two-step method. First,10g of PEG and 5.9g of EL-20 were mixed in a 100-ml three-necked flask under a nitrogen atmosphere and heated at 65 °C, after which 8.38 g of IPDI was added with stirring for 2 h to obtain the prepolymer.

Successively, issolve the gelatin and BDO in deionized water at 40 °C, then mixed with prepolymer, stir the glass rod at high speed for 1 min, the mixture was injected by a syringe, the injectable scaffold would formed at 5–10 min. PU-Foam (PUF) was prepared with 20g of prepolymer and 5g of deionized water; PU-BDO- Foam (PUBF) was prepared with 20g of prepolymer, 5g of deionized water and 0.3g of BDO; PU-Gelatin-Foam (PUGF) was prepared with 20g of prepolymer, 5g of deionized water and 0.5g gelatin; PU-BDO-Gelatin-Foam (PUBGF) was prepared with 20g of P, 5g of deionized water,0.5g of gelatin and 0.3g of BDO. The inject-PUBGF named I-PUBGF, the inject-PUF named I-PUF.

2.3. Characterization method

FT-IR. The molecular structure of the as-prepared materials was characterized using Fourier transform infrared spectroscopy. The sample should be dried in a vacuum drying oven for 24 h to ensure that the sample is fully dried and then tested by infrared spectroscopy. FT-IR operating parameters: scanning range 4000~400 cm^{-1}, resolution 4 cm^{-1}, test temperature 25 °C.

Mechanical compression test. The mechanical properties of PUF, PUBG, PUGF and PUBGF were measured by TA-XT plus Texture Analyzer (Stable Micro Systems, Godalming, UK). The standardization standard by "EN ISO 604–2003: Plastics - Compression Mechanical Properties" is implemented, and the samples are prepared in accordance with the requirements of Class I samples in the standard, scaffold were cut into $30 \times 30 \times 15$ mm^3 dimensions, and 3 specimens were tested according to EN ISO 604–2003 standard with 0.1 mm/min test speed and the temperature is 25 °C, the compression strain is 70%. The number of parallel samples tested was 3. Final compressive young's modulus values were calculated as the slope of the stress-strain curve in the linear region (10 %–15 % of strain) [30].

The mechanical properties of injectable scaffolds were tested by cyclic compression experiment, the mechanical properties of injection scaffolds were tested by TA-XT plus Texture Analyzer. The prepolymer and blowing agent were weighed to 5 g, thoroughly mixed and stirred in a 200 ml beaker for 60s, and the mechanical machine test height was adjusted at the highest liquid level of 0, and the cyclic compression test was carried out. Specimens were tested with 1 mm/s test speed and the temperature is at 20 °C, the mechanical probe test distance is 0 + 40 mm, 500 cycles, each group of samples were tested three times [22].

The density and porosity of the samples were measured by the pycnometer method. The first step is to measure the dry weight of the sample, which is recorded as m$_1$, weigh the mass of the entire pycnometer, and record it as m$_2$. After weighing, proceed to the third step, open the cork, and take out the sample from the pycnometer with tweezers, and use a dry filter paper on one side of the sample to absorb the excess water adsorbed on the surface due to the action of surface tension. The sample is then weighed again, and the measured mass of the sample is recorded as m$_3$, and the mass of the entire pycnometer is weighed and recorded as m$_0$. The number of parallel samples tested was 3.

$$\text{Foam porosity}: P = \frac{V_f}{V_b + V_f} = \frac{m_3 - m_1}{m_0 - m_2 + m_3} \times 100\% \quad (1)$$

In formula (1), m$_1$ is the dry weight of the PUBGF bracket sample, g; m$_2$ is the combined mass of the pycnometer and the sample filled with water, g; m$_3$ is the mass of the cut sample after it is full of water, g; m$_0$ is the mass of the pycnometer filled with water, g.

Measurement of volume change. Due to the closed structure of the sample after molding, the volume of the sample was measured by drainage method. Measurement method refer to the pycnometer method. The number of parallel samples tested was 3.

The samples of each group were analyzed by TG-DTA with a thermogravimetric analyzer. The weight of the test samples was 5–15 mg, the test temperature range was 50–600 °C, the heating rate was 10 °C/min, and the protective gas was nitrogen.

In vitro immersion experiment. The PUF and PUBGF scaffolds were placed in a 37 °C vacuum drying oven to dry to constant weight, and the initial mass of the weighed samples were recorded as M$_1$. The prepared samples were placed in the simulated tissue fluid PBS, the test temperature is a constant 37 °C, and their degradation was observed every 7 days, the degraded samples are also dried and weighed. The mass loss rate during the degradation was calculated [31].

$$\text{Mass loss ratio}: I = (M_2 - M_1)/M_1 \times 100\% \quad (2)$$

In formula (2), M$_1$ is the initial sample mass, g; M$_2$ is the mass after degradation, g. The number of parallel samples tested was 3.

Inject I-PUBGF into a 48-well plate, and after formed, remove the I-PUBGF scaffold. The PUBGF scaffold is then cut into identical cylinder dimensions (diameter: 11 mm, height: 18 mm). Conduct an in vitro degradation experiment in a PBS solution at 37 °C, referring to the cell experiment. The ratio of scaffold to PBS was 0.2 g:1 mL, with testing conducted for 0–15 days, including three parallel samples in each group. After the experiment, collect the degradation solution from both the interior and exterior of the scaffold, and perform quantitative analysis using a BCA assay kit.

Fluid dynamics finite element analysis using Fluent module of Ansys 2022 R1. Establish models of three different surface pores based on actual tested porosity and pore size. The fluid is described using the k-epsilon turbulence model, with an initial flow velocity set at 0.01 m/s. After 1000 steps of calculation to equilibrium, the flow rate and time path of the model are statistically analyzed.

2.4. Cell experiment

The BMSCs were provided by Wuhan Pricella Biotechnology Co., Ltd (Cat NO.: CP-R131). The P0 BMSCs cells extension covered the culture flask reaching more than 80% and cell passage was carried out. First rinse with sterile PBS solution, 1 mL 0.25% trypsin was added and incubated at 37 °C for digestion for 2 min. Finally, 3 mL of BMSCs complete culture medium (89% low glucose Dulbecco's modified Eagle's medium, 10% FBS, and 1% penicillin streptomycin were added to terminate digestion, and the cell suspension was inhaled into a 15 mL centrifuge tube for 1500 rpm for 3 min. After the supernatant was discarded, the culture medium was added to resuscitate the cells. Cells was cultured at 37 °C and 5% CO$_2$ saturation humidity.

BMSCs cells were used to test the safe concentration of the cytotoxicity of scaffolds. The formed scaffolds ($10 \times 10 \times 1$ mm^3) were sterilized with Co-60, for the injectable scaffolds, the prepolymers, deionized water, BDO, and gelatin were sterilized with Co-60 and foamed in a sterile environment prior to cell experiments. The formed scaffolds and DMEM were prepared by the ratio of 0.2 g:1 mL, and the extraction solution was extracted at 37 °C for 24 h, The extract of injectable scaffolds was obtained by direct foaming in DMEM, 37 °C for 10 min. Each experimental group will test 3 parallel samples.

In vitro cytotoxicity of scaffolds was evaluated using CCK-8 (Dojindo, Japan), the extraction solution and scaffold surface culture cells were tested respectively. BMSCs cells (10^5 cells/ml) were seeded in a 96-well plate and were cultured in DMEM with 10% fetal bovine serum (FBS) and 1%penicillin/streptomycin (PS) at 37 °C for 24 h. The 100 μL of culturemedium extracts of PUF, PUBGF, I-PUF and I-PUBGF were added to each of the wells tococulture for 1–3 days. The scaffold was placed in a 48-well plate and BMSCs cells (10^5 cells/ml) were seeded on

the surface of scaffolds for 1–5 days. The medium was changed every 2 days. At each time point, 10 μL CCK-8 solution was added toeach of the wells for 2 h of incubation under cell culture conditions. Each experimental group will test 3 parallel samples.

After incubation for 1–5 days, the cells were stained alive and dead, and then observed with fluorescence microscope (BX-50, Olympus), each experimental group will test 3 parallel samples. At the same time point, cell viability was evaluated with cell counting kit 8 (CCK-8, Dojindo, Japan). At each time point, 10 μL CCK-8 solution was added to each well successively, and OD values were measured at 450 nm using a microporous plate apparatus (MULTISKAN MK 3, Thermoelectron Co., USA). All samples contain three sets of data, and the results are averaged [32].

The BMSCs were resuspended in DMEM supplemented with 10% FBS and 1% penicillin/streptomycin, with a concentration of 5×10^5 cells/ml. The cell suspension was immediately seeded into 24-well plates (1 ml per well) and incubated in a cell culture incubator. Once the cells reached 95% confluence, a straight line was scratched in the center of each well using the tip of a P200 pipette. Subsequently, the cells were washed with sterile PBS to remove detached cells, followed by the addition of culture medium containing PUF and PUBGF extract into each well for 2 days. Next, the BMSCs in each group were kept in the cell culture incubator for 0–48 h, then removed, and photographed using an inverted microscope to assess cell migration activity. Each experimental group will test 3 parallel samples. Calculate the area of scratches using Image-Pro Plus.

The P3 BMSCs cells and chondrogenesis differentiation medium (DMEM, 1% PS, 100 nmol/L dexamethasone, 110 mg/l sodium pyruvate, 50 mM ascorbate 2-phosphate, 100 nmol/L dexamethasone, 23 mg/mL proline, 1% ITS, and 10 ng/mL TGF-β) were used to induce chondrogenesis differentiation. The experiment was carried out for 7–14 days, after which the cells were fixed with paraformaldehyde, and then Alcian blue staining and collagen-II immunohistochemical staining were performed [33].

Alcian blue stain. Cells fixed in 4% polyformaldehyde were washed with PBS for 10 min. The fixed cell layer was then soaked in 3% Alcian blue solution with 37 °C acetic acid (pH 2.5). After staining for 30min, the cells were washed with secondary distilled water. Each experimental group will test 3 parallel samples.

Collagen II staining. Cells fixed in 4% polyformaldehyde were washed with PBS for 10 min and then closed with 5% goat serum for 10 min. The sealing solution was sucked away and the cells were incubated with anti-collagen II (1:400, Abcam, ab34712, China) at 4 °C for 12 h. PBST was cleaned for 10 min, HRP conjugated Goat Anti-Rabbit IgG (H + L) (1:300, Abcam, China) was incubated at room temperature for 45 min, and finally DAB was used for dark color development for 30 min. Each experimental group will test 3 parallel samples. The results of immunohistochemical staining were quantitatively analyzed by Image-Pro Plus. The random field of view was photographed and the average optical density was analyzed [34–36].

2.5. In vivo experiment

The animal experiments conducted as a part of this study were approved by Approval Form of IEC, the Fourth Medical Center of PLA General Hospital, review number:2020KY035-HS001. Male SD rats (200–250 g, 6 weeks, n = 5) were purchased from VitalRiver Laboratory Animal Technology (Beijing, China). The rats were anesthetized with 3% pentobarbital sodium and shaved. The sterilization method of the material is referred to 2.4 Cell experiment.

In the cartilage repair experiment, a 1.5 mm outer diameter trephine drill was employed to create osteochondral defects 2.0 mm in the trochlear groove of the femur. A hole was created inside the defect using a 26-gauge need leand deepened until blood gushed out. And then, in the control group, PUBGF prepared in advance was implanted into the defect, in the experimental group, I-PUBGF was injected into the

cartilage defect, suture the wound after forming. The rats were killed at 1 and 2 weeks, and the blood biochemical test samples were collected and stored according to the test standards, and the automatic biochemical instrument was used for detection. Liver and kidney samples were immediately put into fixed solution for HE staining sections.

After operation, gait analysis were performed at 4 weeks, 8 weeks and 12 weeks. CT and pathological sections of HE, Safranin O-Fast Green and collagen II staining were made at 8 weeks and 12 weeks after operation. The pathological sections were scanned by panoramic scan, and the average optical density of the staining results of the newly born cartilage was counted by Image-Pro Plus.

2.6. Statistical analysis method

Statistical analysis was carried out using SPSS software version 21.0 (SPSS, Chicago, IL, USA). The data were compared using one-way analysis of variance (ANOVA), combined with Dunn's post hoc test. Data are presented as mean ± SD differences were deemed to be statistically significant at $*p < 0.05$, $**p < 0.01$ and $***p < 0.001$.

3. Results and discussion

3.1. Characterization of scaffolds at injection and mold

Upon curing the scaffolds for 1 h, FT-IR tests were conducted (Fig. 2 (a)). All samples showcased the typical polyurethane FTIR characteristics [37,38]: an absorption peak around 1714 cm^{-1} for amide carbonyl (C=O) stretching vibrations, an absorption peak near 1637 cm^{-1} for urethane carbonyl (C=O) stretching vibrations; an absorption peak within the range of 1548 cm^{-1} corresponds to amide bonding; an absorption peak at 1244 cm^{-1} for ester group (C–O) stretching vibrations. In the PUBGF sample, there was no absorption peak at 2270 cm^{-1}, whereas the other three groups of samples exhibited absorption peaks, and with the introduction of gelatin and BDO, the weakening trend of the –NCO absorption peak is quite evident [31,39]. These results indicate that the –NCO is most rapidly reacted upon the injection of PUBGF.

The injectable PUBGF, as illustrated in Fig. 2(b), underwent mechanical characterization under cyclic compression to explore the dynamic proceedings. It can be discerned from the subsequent results, as visualised in Fig. 2(c), that post-injection, all variants of the material exhibited a significant surge in mechanical data. The unmodified PUF projected a concave trend in the course of formation. The snapshots of both PUBF and PUGF samples demonstrated comparable outcomes, presenting marginal fluctuations from the PUF pattern, whereas the PUBGF exemplified a pronounced shift featuring swift accelerations and a convex curve. Deriving the highest derivative twice after fitting the peak values for each cycle, we arrived at Fig. 2(d) and Fig. S2. Each graph presents two inflection points. In accordance to these positions, we segmented the curves into three zones (marked by distinct background colours as regions I, II, III), which components correspond to transitions in the material's physical attributes: liquid phase, rapid expansion, and processing hardening phases [40,41]. Collating data from Fig. 2(c ∼ d), it emerges that following its foaming initiation, PUF's liquid phase persisted for 149s, subsequently entering into a rapid expansion phase spanning across 980s, thereby totalling to a duration of 1129s. Meanwhile, the modified variant, PUBGF, maintained its liquid phase for 119s, and after navigating through 668s, it commenced the processing hardening stage. The combined duration for these two phases amounted to 787s. The degree of change in the volume of the material was in direct proportion to the mechanical data. Across the entire experimental timescale, PUF documented a 3125.8% change in volume, while the process of volume expansion was yet to cease at the end of the testing period. Conversely, PUBGF reached its maximum value of 2728.3% at roughly 900 s and then incurred a slight decrease in volume, thereby suggesting that the foaming reaction for this specimen had practically culminated at 900 s, as depicted in Fig. 2(f).
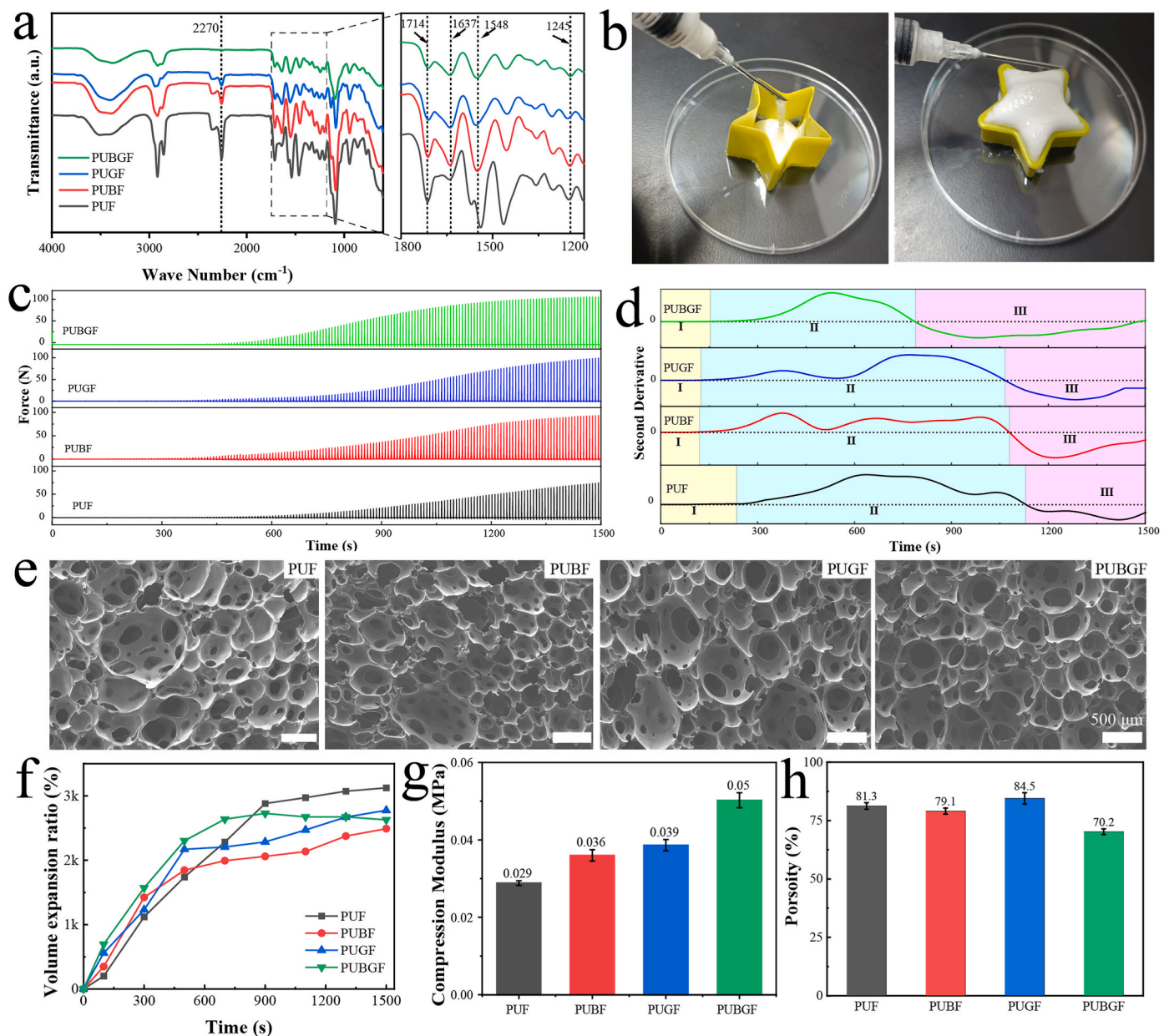
Fig. 2. (a) FT-IR. (b) The injectivity and formability of I-PUBGF. (c) Cyclic compression performance. (d) The 2nd derivative of collected cyclic compression data. (e) Surface morphology of different samples. Scale bar: 500 μm. (f) Volume expansion ratio after injected. (g) Compressive young's modulus. (h) porosity.

The microscopic morphology of each group's PUBGF porous scaffold is shown in Fig. 2(e). As can be seen, the pores of the scaffold are mostly circular, with good connectivity between cells, which facilitates the circulation of cells and tissue fluid in the body. The SEM images revealed that the composition of the foaming agent affects the pore size of the sample. The pores of the PUBGF scaffold are uniform and relatively small, while the other three groups have larger pores similar to defects. This outcome has affected the porosity of the scaffold (Fig. 2(h)). The porosity of PUGF, PUF, and PUBF samples are all greater than 80%, but the porosity of PUBGF has reduced to 70.2%. Fig. 2(g) presents the compressive mechanical properties of each group's molded samples. Compared to PUF, both the Young's modulus of PUBF and PUGF have improved to some extent, but the mechanical properties of PUBGF have increased significantly.

During the execution of animal surgery, the liquid phase of PUBGF can be capitalized on for injections, whilst its solid phase can seal wounds, clearly establishing PUBGF as a rather fitting substance to

utilise. In addition, an hour post its formation, the –NCO within PUBGF undergoes a complete reaction, resulting in a microscopic structure or mechanical characteristics that makes it the most suitable material for injectable scaffolds.

3.2. In vitro degradation test

In-vitro degradation experiments of PUF and PUBGF scaffolds post-injection were conducted, with a particular emphasis on variations in the materials' microscopic structure. As illustrated in Fig. 3(a), PUF showcases a distinctly lower weight loss rate compared to PUBGF, in which the degradation is observed to be in an accelerated state, indicating the continued influence of the gelatin linkages present within PUBGF on its degradation process [42]. Residues post-degradation were subjected to TG testing, the findings from DTG and TG presented in Fig. 3(b and c). It can be inferred that following its degradation, a minute decomposition peak roughly at 150 °C in PUBGF gradually vanishes,
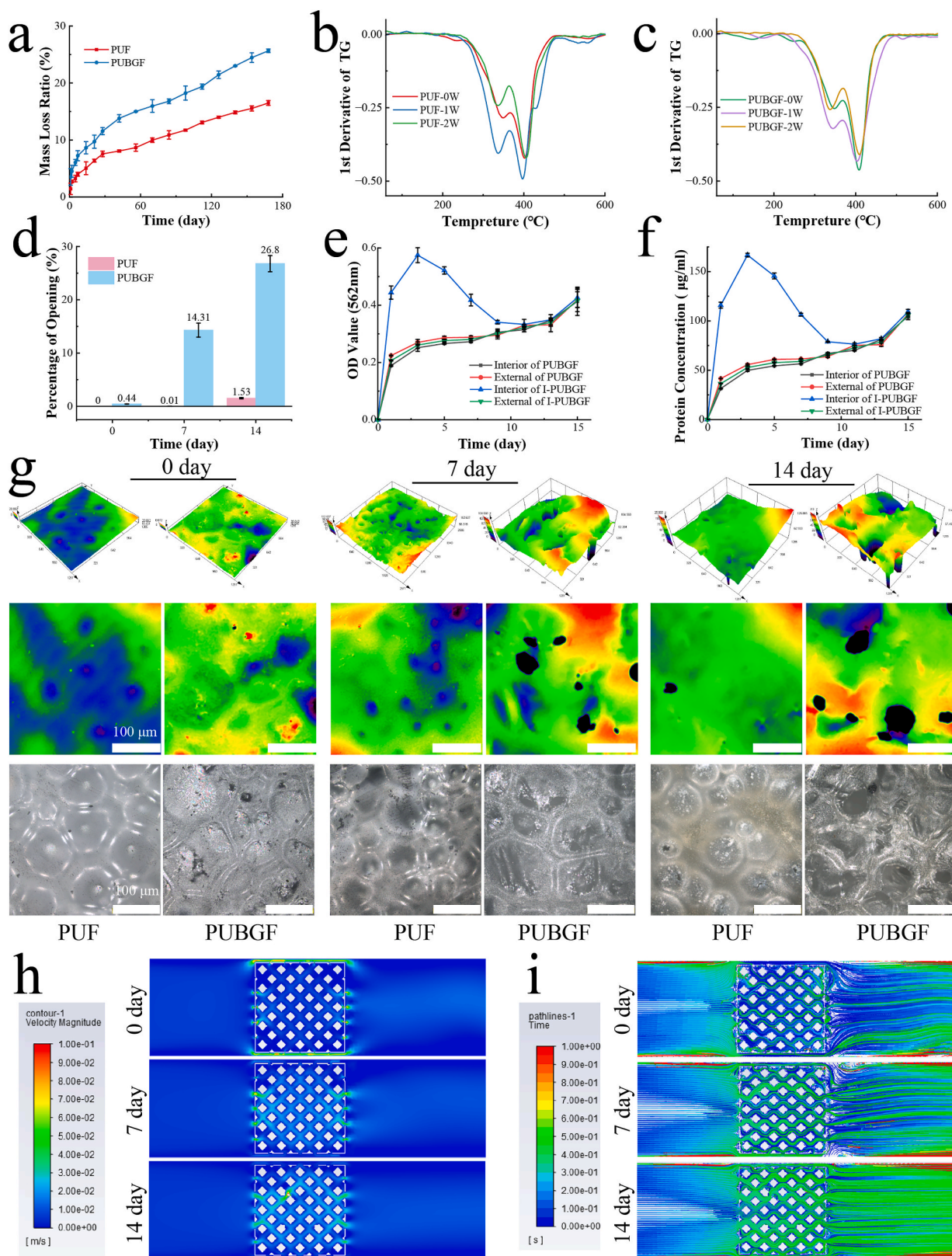
Fig. 3. (a) Weight loss rate of samples immersed in PBS for 180 days. (b) DTG curves of PUF after immersing in PBS for 2 weeks. (c) DTG curves of PUBGF after immersing in PBS for 2 weeks. (d) Opening rate of outermost layer of PUF and PUBGF within 2 weeks; (e) OD levels of protein concentration inside and outside the scaffold within two weeks. (f) Levels of protein concentration released inside and outside the scaffold within two weeks. (g) 3D surface morphology, surface plane projection topography and surface optical morphology of different materials. Finite element analysis (FEM) of (h) flow velocity and (i) time pathline for scaffolds with surface pores of different sizes. Scale bar: 100 μm. Data are presented as mean ± SD(n = 3).

showing noticeable similarity with PUG around the fortnight mark, the gelatin segments within PUBGF have been extensively degraded.

Our investigation primarily focused on the distinct contrasts observed between the degradation profiles of directly injected scaffolds and conventional ones in terms of substance retention. Inject-PUBGF (I-PUBGF) was administered via injection into a vessel to conduct degradation assays, while its counterpart, comprised of PUBGF precisely cut into uniform shapes, was subjected to a collection regime every two days; this involved gathering the degradation fluid both from within the scaffold and diffused externally. The BCA assay was utilized to measure protein concentration, revealing a notably stark difference during the initial 10-day period, as depicted in Fig. 3 (e, f). Insights garnered from the extrapolated protein concentration data indicate that the degradation products of the I-PUBGF scaffold—specifically, the gelatin segments—were predominantly retained within the scaffold. At their peak, the internal protein concentration was threefold higher than that externally, eventually declining to levels commensurate with those of I-PUBGF. Conversely, the PUBGF lacked this characteristic retention; devoid of any sealed outer structure, its degradation products dispersed directly into the surrounding medium [18].

The ultrastructural architecture of the scaffold's outermost layer was characterized using a laser confocal microscope, as depicted in Fig. 3 (d–g). Upon formation, both the PUF and PUBGF initially exhibited a predominantly sealed outer surface. After one week of degradation, a quantifiable proliferation of pores was observed in the PUBGF, with a continued increase in the number of pores reaching an open area of 26.8% and pore diameters exceeding 50 μm by the second week. Conversely, the PUF displayed negligible alterations [25,42,43].

Using finite element analysis of fluid mechanics, simulations were conducted to contrast the flow of degradable substances through materials with static apertures versus those with dynamic, changing orifices, namely PUBGF and I-PUBGF. Results indicate that substances face difficulties flowing through the interior of materials when surface pores are small. Furthermore, substances cannot penetrate the interior of materials to a significant degree when flowing through the edges. As the control increases, the material flows rapidly into the pores with lower flow velocity in the middle, facilitating material retention. Further increase in pore size allows the whole fluid to easily pass through the pores (Fig. 3(h)). The graph illustrates the time taken by the fluid to traverse various regions. As porosity increases, a substantial quantity of material gets deposited in the pores (Fig. 3(i)). This indicates a lack of communication between the material's internal and external environments during the initial stages of repair, thereby providing evidence to support the retention of substances such as gelatin within the material. Over time, external substances penetrate the material and persist in the surrounding environment, contributing to a constant build-up of substances used for tissue repair.

Degradation studies indicate that upon being injected into the physiological environment, the outermost structure of I-PUBGF gradually transitions from a closed to an open state. During this process, substantial amounts of degraded gelatin and other substances are retained within the scaffold, which evidently provides considerable advantages for cartilage regeneration.

3.3. Cell experiment

As a long-term implant, it is essential to conduct cytotoxicity experiments on the materials. The study simulates animal experiments testing Inject-PUF (I-PUF) and Inject-PUBGF (I-PUBGF), as well as the cured materials PUF and PUBGF. Fig. 4(a) demonstrates the impact of the extracts on cells during the material foaming process and after curing, culturing BMSCs cells on scaffold surfaces and in the extracts, performing live/dead staining and F-actin staining, and evaluating cell proliferation via the CCK8 test. The number of living green cells in the I-PUF group is much lower than other groups, and F-actin staining displays cells with a round morphology in the I-PUF group. The I-PUBGF

group performs well, exhibiting similarities in outcomes with the cured PUF and PUBGF [44], displaying an abundance of live cells in live/dead staining, few red dead cells, while F-actin staining reveals large cell spreading areas and pseudopods, indicating a favorable cell growth status. The cell cytotoxicity of the CCK-8 results from co-culturing material extracts and surfaces is presented in Fig. 4(b and c), consistent with the conclusions of the cell staining; I-PUBGF exhibits no significant cytotoxicity.

Cell migration is a necessary prerequisite for scaffold-mediated tissue repair, as it can promote the migration, differentiation, and proliferation of stem cells. In this study, the migratory capacity of cells was assessed via a wound healing assay. The experimental outcomes, depicted in Fig. 4d and f, reveal that at the 48-h mark, PUF exerts negligible influence on the BMSCs. In contrast, BMSCs cultured with PUBGF exhibited superior migratory capabilities compared to both the control and PUF groups. Statistical analysis demonstrates that the scratch area in the PUBGF group was consistently and significantly smaller than that in the other groups across all time points measured. In summary, the PUBGF scaffold may enhance the adhesion, proliferation, and migration of BMSCs, potentially playing a remarkable role in cartilage repair [45].

The experimental group consisted of co-cultures of PUF and PUBGF scaffolds with P3 BMSCs cells, while the control group did not include any scaffolds, and Alcian Blue staining and collagen II staining are implemented after 7–14 days to investigate the scaffold's potential for chondrogenic differentiation. It can be observed from Fig. 4(g) that there are no significant differences in the two staining results between the control group and the PUF group. However, a remarkable distinction is noticeable for the PUBGF group at 7 days, with the staining area far exceeding PUF and control, and the disparity is further widened at 14 days. Upon analysis of the average optical density statistics for the immunohistochemistry results (Fig. 4(e)), it was evident that the accumulation of collagen II near the cells cultured with the PUF scaffold was not significantly increased compared to the control group. Conversely, the PUBGF group exhibited an enhancement of 83% and 60.7% over the control and PUF groups, respectively, indicating a commendable proficiency in promoting cartilage repair. Undoubtedly, PUBGF has a significant promotional effect on chondrogenic differentiation.

To further study the potential of PUBGF on chondrogenic differentiation, Q-PCR and the expression of cartilage-specific genes are evaluated. Significant increases are observed in the mRNA expression levels of cartilage-specific genes collagen II (Col 2), aggrecan (ACAN), and Collagen X, with a modest increase in Sox9 protein expression as shown in Fig. 4(f). In comparison, the cartilage-specific gene expression levels in the PUF group exhibit only a slight elevation over the control group and are all lower than those in the PUBGF group [46].

3.4. Cartilage repair experiment

In an experimental procedure, an irregular cylindrical defect with a 2 mm diameter and 1.5 mm depth was created in the condylar groove of the femoral trochlea of rats. The materials, including I-PUBGF, were directly injected, solidified, and the wound was subsequently sutured. Cylindrical PUBGF grafts were carved and implanted, directly followed by wound suture. Meanwhile, the control group received no scaffold implantation. Gait analysis was performed postoperatively, and at the 12-week mark, a CT scan was conducted. The animal model is depicted in Fig. 5(a).

Postoperative gait analysis experiments were conducted on each group of rats every four weeks, as depicted in Fig. 5(b–d). Representative footprints and stance/swing images of each group of rats can be seen in Figure d. The lengths of the first to fifth toes (TS), second to fourth toes (IT), and third toe to heel (PL) were measured on the operated and contralateral normal sides, with the non-operated left hind limb serving as the healthy foot control group. It can be observed that at 4–8 weeks, the footprints of the I-PUBGF group resemble those of the non-operated footprints, with the operated limbs landing on the heel and toes,
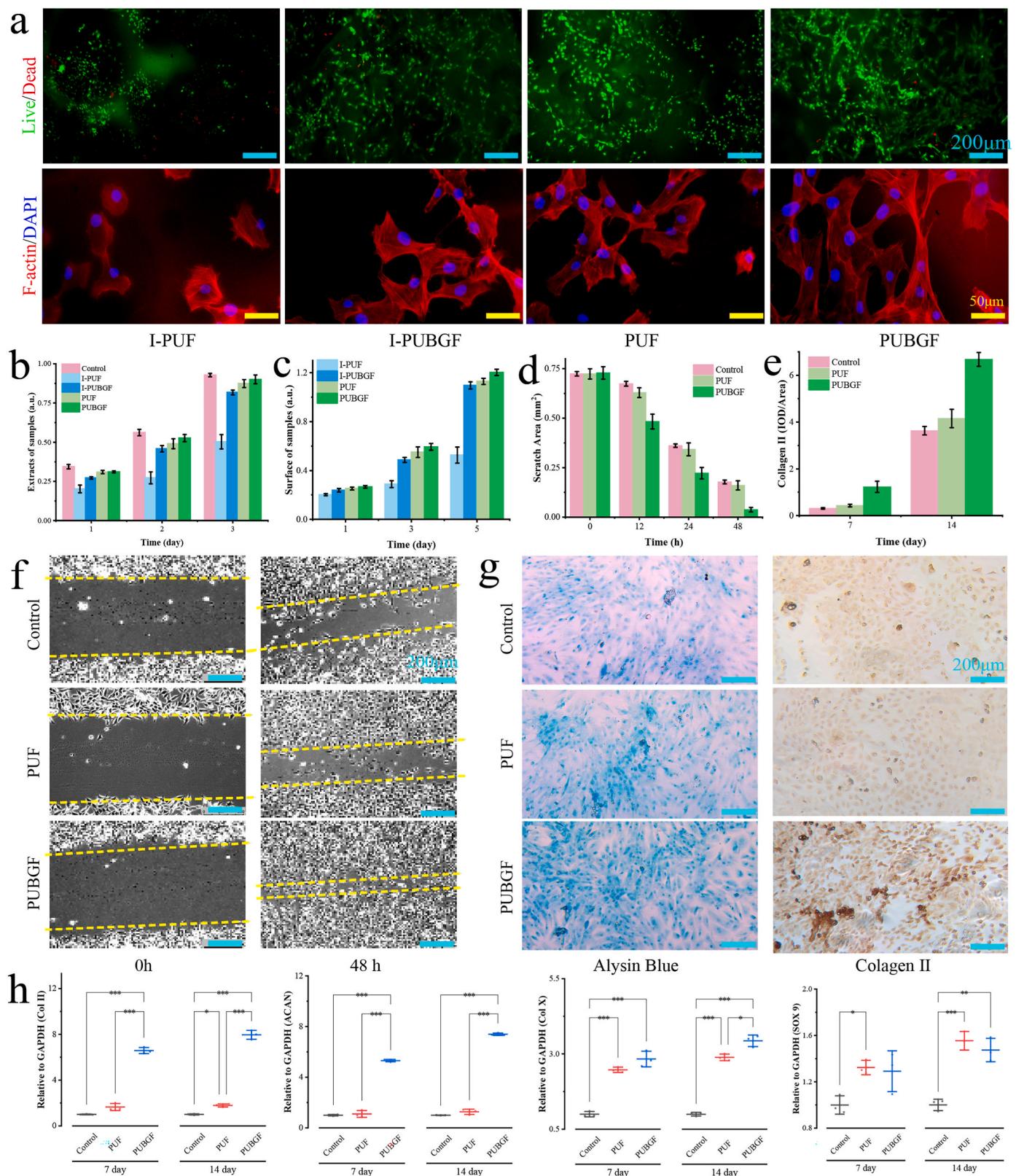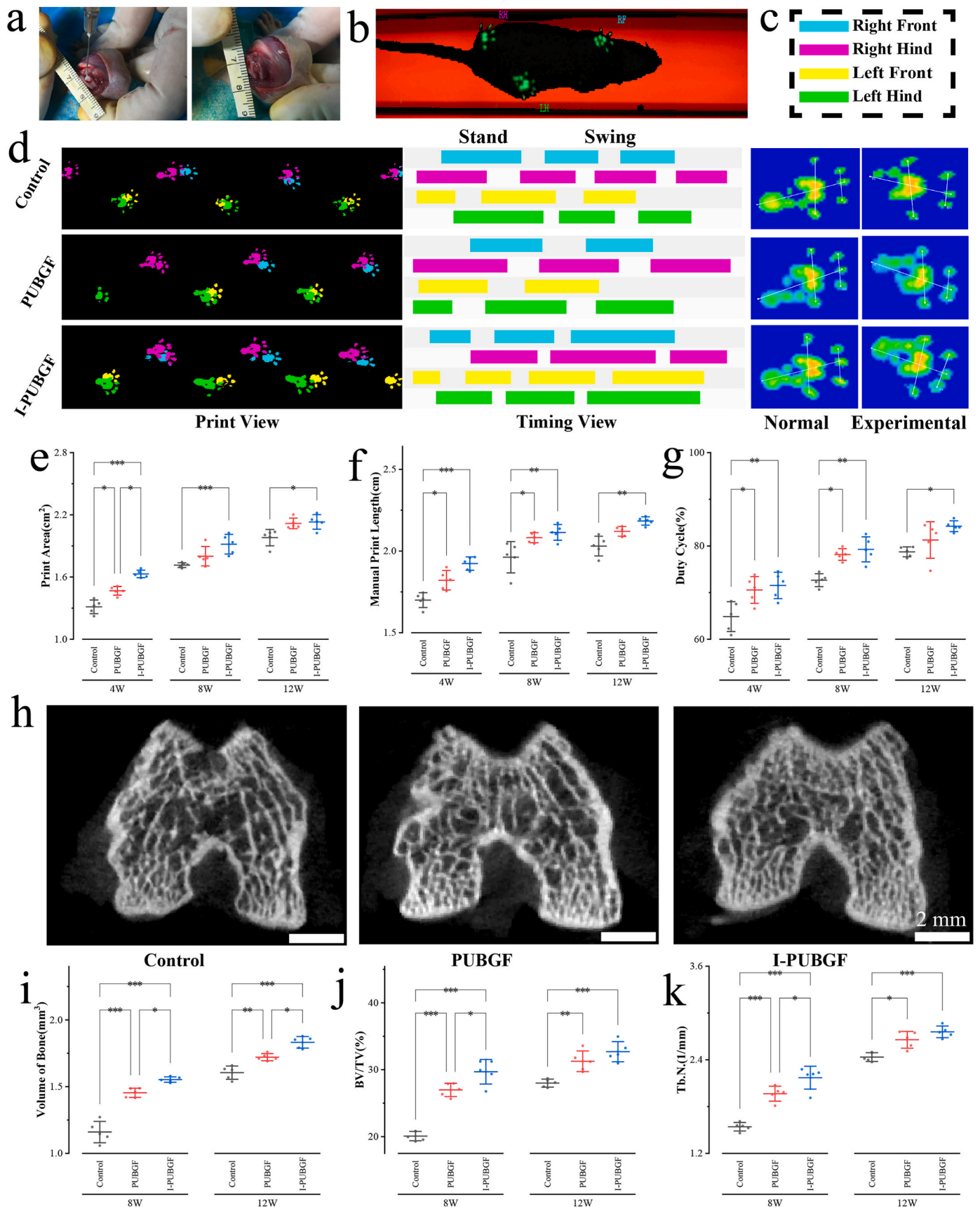
Fig. 4. (a) Live/dead staining and phalloidin staining of cells after culturing on the material surface for 3 days. (b) CCK-8 test of cells after culturing in material extract. (c) CCK-8 test of cells after culturing on the material surface. (d) The result of wound healing. (e) Immunohistochemical analysis of Collagen II in vitro chondrogenic differentiation. (f) Wound healing. (g) Chondrogenic differentiation for 2 weeks, with staining results of Alisin Blue and Collagen II. (h) mRNA expression of the cartilage-specific genes, Col II, Col X, Acan, and Sox9 in the control and experimental groups based on Q-PCR. Blue scale: 200 μm; Yellow scale: 50 μm. Data are presented as mean $\pm$ SD (n = 3, *p < 0.05, **p < 0.01, ***p < 0.001).

Fig. 5. (a)Cartilage defect creation and scaffold implantation. (b) Example of classified footprints in an image collected from the videos captured. (c) Legend of footprints. (d) Print view, Timing view and Foot print of CatWalk. (e)~(g) Print area, Manual print length and Duty cycle of CatWalk. (h) image of CT. (i) Volume of bone; (j) Bone volume fraction, BV/TV (k) Trabecular number, Tb·N. White scale: 2 mm. Data are presented as mean ± SD (n = 5, *p < 0.05, **p < 0.01, ***p < 0.001).

demonstrating a significant improvement compared to the primarily heel landing PUBGF group and control group. At 12 weeks, the I-PUBGF group still outperforms the other two groups, albeit with a smaller margin. Similar results are observed in the stance/swing images. From Fig. 5(e and f), it is evident that the footprints statistical data of the I-PUBGF group significantly outperforms the control group, and also surpasses the PUBGF group. The Duty Cycle statistical results indicate that in the fourth week, the stance/swing data of the I-PUBGF group is 71.53% ± 2.82%, while the PUBGF group and control group are 70.56% ± 2.86% and 64.86% ± 3.19%, respectively. All three experimental groups recover to around 80% by the twelfth week post-surgery. Gait testing is primarily affected by postoperative pain, as well as the imbalance of stress in the surrounding tissue caused by the wound, for which the implantation of the scaffold can help improve. Therefore, both the PUBGF group and I-PUBGF group exhibit superior gait testing results compared to the control group. Compared to the two experimental groups with implants, the I-PUBGF scaffold can be shaped in situ, perfectly matching the shape of the wound. This allows for more balanced stress between the scaffold and surrounding tissue, resulting in better recovery and lower pain perception. Hence, the I-PUBGF data surpasses the PUBGF group. In the later stages after surgery, the defect site is filled with newly generated tissue. However, due to the lack of neural tissue in the knee joint cartilage, there is not much difference in the data among the groups. Nevertheless, the reconstruction speed and effectiveness of the tissue in the early stages influence the testing results, affirming that the repair effect of I-PUBGF on rat articular cartilage is superior.

Fig. 5(h) presents the 12-week post-repair CT images of rat femoral condyles. It is apparent that the cartilage and subchondral bone structure at the trochlear groove are intact in the groups with PUBGF and I-PUBGF scaffolds, in contrast to the evident subchondral bone defects in the control group. The statistical CT outcomes for each group are shown in Fig. 5(i ~ k), where the bone tissue CT parameters of a 2 mm diameter, 1 mm depth zone at the trochlear groove defect site have been analyzed. The statistical data of subchondral bone in rats from both the PUBGF and I-PUBGF groups substantially outperforms that of the control group, most notably within the initial 8 weeks. It suggests that the space at the defect site was rapidly filled with new bone tissue, while the rate of bone repair was slower in the control group, which may be attributed to the microstructure and chemical composition of the materials enhancing bone tissue repair. Between 8 and 12 weeks, the subchondral bone in the I-PUBGF and PUBGF groups had almost reached the normal bone tissue state, hence the sluggish growth in data. Comparative analysis of I-PUBGF and PUBGF group data indicates that the in situ formed I-PUBGF scaffolds are more conducive to subchondral bone reconstruction [47].

The restoration of bone tissue is influenced by various factors, with mechanical stimulation being significant. The I-PUBGF better conforms to the shape of the defect, leading to more uniform mechanical transmission in the joint cartilage, and preventing localized stress concentrations, which results in superior gait analysis and CT test outcomes for the I-PUBGF group when compared with the PUBGF group.

Histological examination with H&E staining was conducted on rat knee joints at 1–2 weeks post-surgery to ascertain whether the I-PUBGF scaffold maintained a dynamic microstructure at the articular cartilage site and to determine if newly formed tissue could seamlessly infiltrate the scaffold. Concurrently, metabolic toxicity of I-PUBGF was assessed through hepatic and renal blood biochemistry tests, with the aid of H&E staining of liver and kidney tissues for supportive evaluation.

Fig. 6(a) reveals that a modest amount of tissue had penetrated the interior of the I-PUBGF after one week. By the two-week mark, an abundance of tissue was evident within the scaffold, achieving
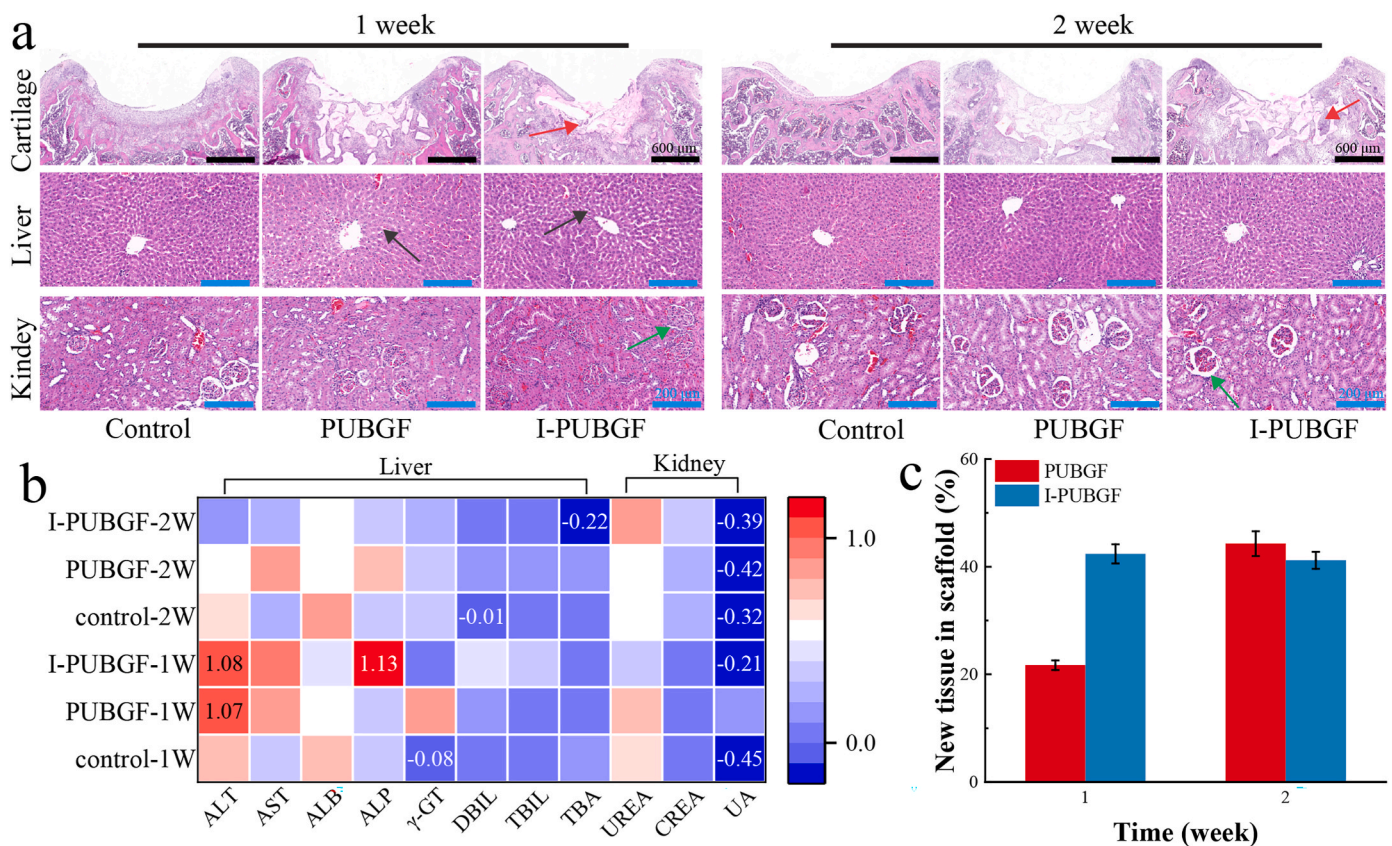

Fig. 6. (a) HE staining of knee joint, liver and kidney was performed 1–2 weeks after operation. (b) 1–2 weeks after the operation, the rats' blood biochemical tests were performed, and the test results were normalized. (c) New tissue in scaffolds. Black scale: 600 μm, Blue scale: 200 μm. Red arrow, new tissue in the scaffolds. Black arrows, disordered hepatic cords. Green arrow, glomerular sac. Data are presented as mean ± SD (n = 5, *p < 0.05, **p < 0.01, ***p < 0.001).

infiltrations of 21.2% and 42.5%, respectively, indicating that I-PUBGF retains a dynamic microstructure *in vivo* and by the second week closely resembles the morphology of PUBGF. Moreover, inflammatory cells were observable in the three experimental groups after one week, which had largely subsided by the second week, further suggesting the favorable biocompatibility of I-PUBGF.

Pathological examination of rat liver sections, as shown in Fig. 6(a), indicates that compared to the control group, the liver lobule architecture appeared relatively normal in rats implanted with I-PUBGF for one week, although the hepatic plates were slightly disordered. After two weeks, the liver lobule morphology was entirely normal, with radially arranged hepatic plates around the central vein and clear hepatic sinusoids, and the portal tract morphology within the field of view appeared

normal. Similar phenomena were observed in the PUBGF group. Renal H&E staining results demonstrate minimal capsular space within the glomeruli for both PUBGF and I-PUBGF groups at one week; by two weeks, the morphology of the nephrons in both experimental groups had improved, correlating with the blood biochemistry findings [48,49].

As depicted in Fig. 6(b) and Table S1~S2, findings from the biochemical analysis of rat blood are presented post-normalization of the testing data. Evidently, the intraperitoneal injection of I-PUBGF does not significantly impact the liver function in rats, with marginally elevated values of ALP and ALT subsequently returning to the norm within a fortnight. Conversely, the Uric Acid (UA) levels of the kidney consistently fell below the standard range, whilst the remaining data points maintained within a reasonable range. A slight deviance in a
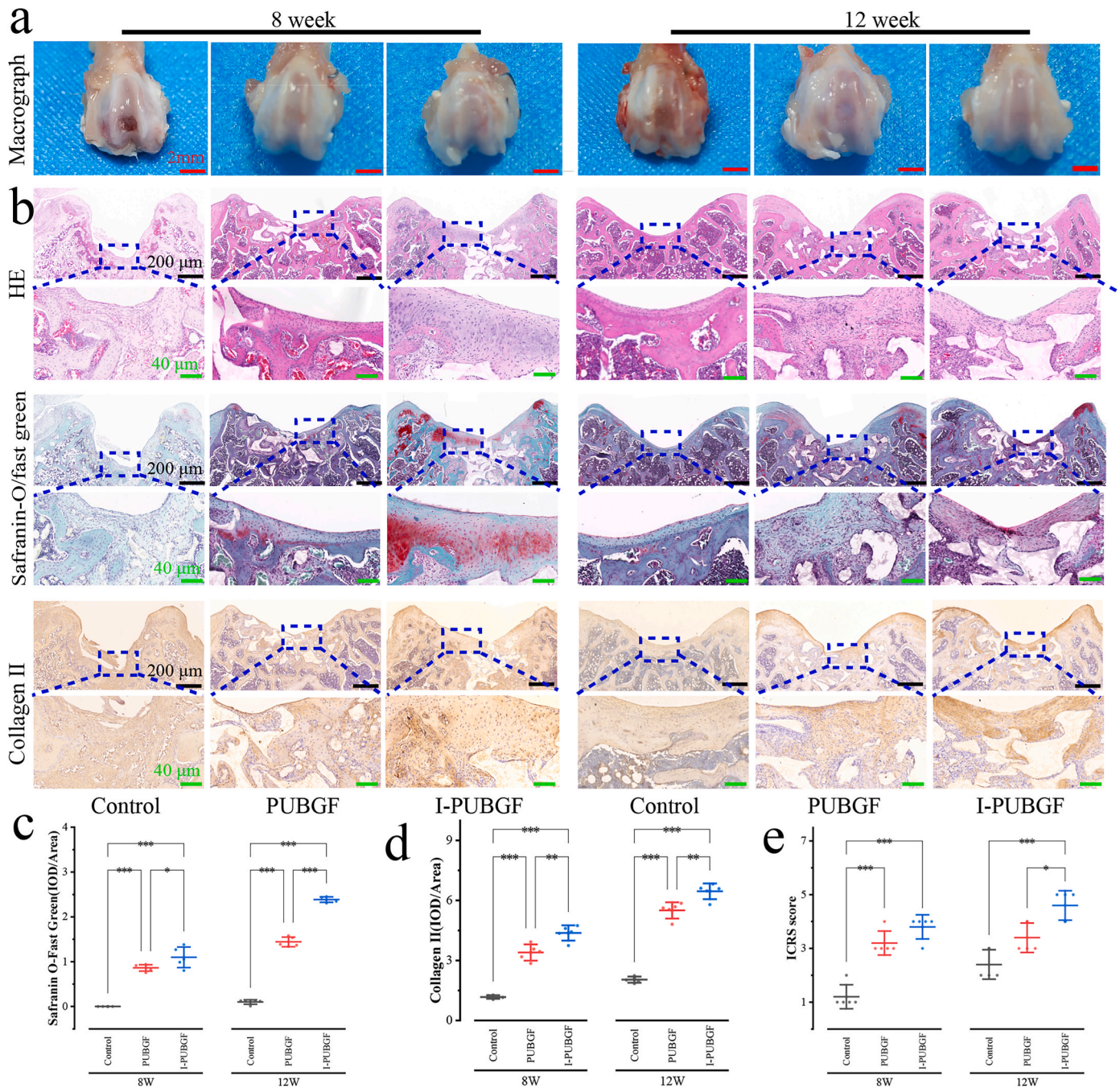

Fig. 7. (a) Macrograph of the specimens harvested at 8 and 12 weeks after surgery. (a) HE staining, Safranin O-Fast Green Staining, Collagen II staining at 8 and 12 weeks after surgery. (c) Average optical density of Safranin O-Fast Green Staining; (d) Average optical density of collagen II staining. (e) ICRS score. Black scale: 200 μm, Green scale: 40 μm, Red scale: 2 mm. Data are presented as mean ± SD (n = 5, *p < 0.05, **p < 0.01, ***p < 0.001).

singular biochemical indicator does not necessarily imply damage to the liver or kidney. The elevation of ALP conjoined with a decrease in ALT has the potential to indicate cellular damage. In this particular experiment, though, the synchronous increase of both anticipates a certain influence of the material on the liver, yet the actual causus belli could most likely be external factors. Typically, dietary intake dictates the natural numerical fluctuations in kidney UA levels, hence a lower value is frequently observed in similar animal testing. When further examined in connection with Fig. 5(a), it substantiates that the in-situ molding of I-PUBGF in the region of joint cartilage defects is indeed safe and does not yield adverse effects.

As illustrated in Fig. 7(a), at 8 weeks post-repair, the cartilage defect areas in the Control group remained substantially wounded, characterized by large and comparatively deep lesions with scant evidence of healing. The defect sites in both the PUBGF and I-PUBGF groups were almost entirely filled by neotissue, although the surfaces were irregular and the demarcation from the surrounding normal articular cartilage remained distinctly visible, with both groups exhibiting similar repair outcomes. At 12 weeks post-repair, the control group's defect areas exhibited an abundance of neotissue with uneven surfaces, and the boundaries between these and the adjacent normal cartilage were sharply defined. The degree of repair in the PUBGF and I-PUBGF groups was superior to that at 8 weeks post-repair, with less discernible differences from the surrounding healthy cartilage; the regenerative results between PUBGF and I-PUBGF groups were remarkably similar, although the morphological repair appeared slightly more advanced in the I-PUBGF group. The ICRS scoring of cartilage in the three cohorts, as depicted in Fig. 7(e), unambiguously demonstrated that both scaffold-reinforced PUBGF and I-PUBGF groups were greatly superior to the control group, with I-PUBGF scoring marginally higher than PUBGF.

Fig. 7 (b) displays the results of staining with Hematoxylin and Eosin (HE), Safranin O-Fast Green, and type II collagen. The positive area results of Safranin O-Fast Green and type II collagen staining can be seen in Fig. 7(c and d). Upon examining the HE staining results, it is evident that the control group exhibited obvious repair failure. At 8 weeks, the defect area was highly pronounced, and no morphological evidence of cartilage tissue could be discerned at 12 weeks. The differences between the PUBGF group and the I-PUBGF group were minimal, as both were able to rapidly fill the defect tissue. Safranin O-Fast Green and type II collagen staining provided a more precise reflection of cartilage repair status. In the control group, the staining results showed barely any positive staining. In the PUBGF group and the I-PUBGF group, the Safranin O-Fast Green staining exhibited minimal differences at 8 weeks, but at 12 weeks, the red-colored newly formed collagen area in the I-PUBGF group was notably larger, with an average optical density value of 2.38 ± 0.06, compared to 1.44 ± 0.11 in the PUBGF group. Type II collagen staining also effectively demonstrated the cartilage repair outcomes in the PUBGF group and the I-PUBGF group. At 8 weeks, the I-PUBGF group exhibited a uniform positive region in the cartilage surface, while the PUBGF group appeared disorganized and had a thinner layer. At 12 weeks, the positive area in the I-PUBGF group was more balanced and extensive, whereas the positive area in the PUBGF group started to exhibit balance but still remained lower than that of the I-PUBGF group. The statistical analysis of the average optical density values for type II collagen staining provided a more contrasting result. Between 8 and 12 weeks, the values for the PUBGF group increased from 3.49 ± 0.4 to 5.50 ± 0.41, while the values for the I-PUBGF group increased from 4.37 ± 0.38 to 6.45 ± 0.35, consistently surpassing those of the PUBGF group at each time point.

The chemical composition and physical properties of the PUBGF and I-PUBGF stents are almost identical, but the repair effect of I-PUBGF is superior to that of the PUBGF group. *In vitro* degradation experiments have shown that I-PUBGF stents have a significantly higher retention capacity of degradation materials in the first two weeks. This is mainly due to the retention of gelatin within the stent after degradation, which has a very significant promoting effect on cartilage repair. Additionally,

I-PUBGF can be formed in situ at the defect site after injection, perfectly matching the shape of the defect site. Compared to the PUBGF stent, the stress distribution after implantation of the I-PUBGF stent is more balanced. These factors contribute to the better repair effect of I-PUBGF.

4. Conclusion

We have engineered an injectable PUBGF scaffold that can adaptively in-situ form a porous framework upon administration. Procuring a dynamic microstructure in the material, through the cross-linking of gelatin and BDO, which facilitates a commendable amelioration in cartilage repair. The absence of residual –NCO in PUBGF after forming was substantiated through FT-IR. *In vitro* degradation experiment demonstrates the dynamic microstructured scaffold, where the closed structure of the scaffold is progressively unveiled. During this process, substances such as gelatin residue within the scaffold is three times that outside. Cellular experiments denote that direct injection of PUBGF exhibits insignificant cytotoxicity, whereas PUBGF significantly stimulates chondrogenic differentiation. Ultimately, by directly injecting PUBGF scaffold into deficient cartilage regions in rats' knee joints, the outcomes revealed normal liver and kidney within $1 \sim 2$ weeks after surgery, with the blood biochemistry data within the customary standards. Rats with injected PUBGF scaffold manifest superior results in CT and gait test, demonstrating a conspicuous effect in cartilage repair. Through the auspices of these findings, we anticipate that PUBGF's dynamic microstructure and injectability withhold immense potential application in joint cartilage regeneration.

CRediT authorship contribution statement

Abudureheman Bahatibieke: Writing – review & editing, Writing – original draft, Visualization, Validation, Software, Resources, Methodology, Formal analysis, Data curation. **Shuai Wei:** Methodology. **Han Feng:** Methodology. **Jianming Zhao:** Visualization. **Mengjiao Ma:** Software. **Junfei Li:** Software. **Yajie Xie:** Resources. **Kun Qiao:** Investigation. **Yanseng Wang:** Writing – original draft. **Jiang Peng:** Project administration, Funding acquisition. **Haoye Meng:** Writing – original draft, Funding acquisition. **Yudong Zheng:** Writing – review & editing, Validation, Supervision, Investigation, Funding acquisition, Conceptualization.

Declaration of competing interest

There are no conflicts to declare.

Appendix A. Supplementary data

Supplementary data to this article can be found online at https://doi.org/10.1016/j.bioactmat.2024.03.012.

References

[1] M. Khoshgoftar, P.A. Torzilli, S.A. Maher, Influence of the pericellular and extracellular matrix structural properties on chondrocyte mechanics, J. Orthop. Res. 36 (2) (2018) 721–729.

[2] Y. Wang, R.F. Pereira, C. Peach, B. Huang, C. Vyas, P. Bartolo, Robotic in situ bioprinting for cartilage tissue engineering, Int. J. Extreme Manuf. 5 (3) (2023) 32004, 2023-1-1.

[3] C.D. O'Connell, S. Duchi, C. Onofrillo, L.M. Caballero-Aguilar, A. Trengove, S. E. Doyle, et al., Within or without you? A perspective comparing in situ and ex situ tissue engineering strategies for articular cartilage repair, Adv. Healthc. Mater 11 (24) (2022) 2201305, 2022-12-1.

[4] H. Kwon, W.E. Brown, C.A. Lee, D. Wang, N. Paschos, J.C. Hu, et al., Surgical and tissue engineering strategies for articular cartilage and meniscus repair, Nat. Rev. Rheumatol. 15 (9) (2019) 550–570, 2019-9-1.

[5] T. Mawatari, D.P. Lindsey, A.H.S. Harris, S.B. Goodman, W.J. Maloney, R.L. Smith, Effects of tensile strain and fluid flow on osteoarthritic human chondrocyte metabolism in vitro, J. Orthop. Res. 28 (7) (2010) 907–913.

[6] L. Zhou, P. Guo, M. D`Este, W. Tong, J. Xu, H. Yao, et al., Functionalized hydrogels for articular cartilage tissue engineering, Engineering 13 (2022) 71–90.

[7] K. Ren, C. He, C. Xiao, G. Li, X. Chen, Injectable glycopolypeptide hydrogels as biomimetic scaffolds for cartilage tissue engineering, Biomaterials 51 (2015) 238–249.

[8] Y. Hua, H. Xia, L. Jia, J. Zhao, D. Zhao, X. Yan, et al., Ultrafast, tough, and adhesive hydrogel based on hybrid photocrosslinking for articular cartilage repair in water-filled arthroscopy, Sci. Adv. 7 (35) (2021), 2021-8-27.

[9] M. Liu, X. Zeng, C. Ma, H. Yi, Z. Ali, X. Mou, et al., Injectable hydrogels for cartilage and bone tissue engineering, Bone Res. 5 (2) (2017) 75–94, 2017-1-1.

[10] M.Y. Ha, D.H. Yang, S.J. You, H.J. Kim, H.J. Chun, In-situ forming injectable GFOGER-conjugated BMSCs-laden hydrogels for osteochondral regeneration, NPJ Regen. Med. 8 (1) (2023) 2, 2023-1-6.

[11] J. Louf, N.B. Lu, M.G. O Connell, H.J. Cho, S.S. Datta, Under pressure: hydrogel swelling in a granular medium, Sci. Adv. 7 (7) (2021) eabd2711, 2021-2-12.

[12] N.R. Richbourg, M. Wancura, A.E. Gilchrist, S. Toubbeh, B.A.C. Harley, E. Cosgriff-Hernandez, et al., Precise control of synthetic hydrogel network structure via linear, independent synthesis-swelling relationships, Sci. Adv. 7 (7) (2021) eabe3245, 2021-2-12.

[13] H. Kamata, Y. Akagi, Y. Kayasuga-Kariya, U. Chung, T. Sakai, "Nonswellable" hydrogel without mechanical hysteresis, Science 343 (6173) (2014) 873–875.

[14] S. Xu, Z. Zhou, Z. Liu, P. Sharma, Concurrent stiffening and softening in hydrogels under dehydration, Sci. Adv. 9 (1) (2023) eade3240, 2023-1-4.

[15] L.J. Eggermont, Z.J. Rogers, T. Colombani, A. Memic, S.A. Bencherif, Injectable cryogels for biomedical applications, Trends Biotechnol. 38 (4) (2020) 418–431.

[16] Y. He, Y. Zhao, L. Fan, X. Wang, M. Duan, H. Wang, et al., Injectable affinity and remote magnetothermal effects of Bi-based alloy for long-term bone defect repair and analgesia, Adv. Sci. 8 (14) (2021) 2100719.

[17] C.F. Guimarães, A.P. Marques, R.L. Reis, Pushing the natural frontier: progress on the integration of biomaterial cues towards combinatorial biofabrication and tissue engineering, Adv. Mater. 34 (33) (2022) 2105645.

[18] Y. Wang, X. Yuan, K. Yu, H. Meng, Y. Zheng, J. Peng, et al., Fabrication of nanofibrous microcarriers mimicking extracellular matrix for functional microtissue formation and cartilage regeneration, Biomaterials 171 (2018) 118–132.

[19] L. Zhu, D. Luo, Y. Liu, Effect of the nano/microscale structure of biomaterial scaffolds on bone regeneration, Int. J. Oral Sci. 12 (1) (2020) 6, 2020-2-6.

[20] M.G. Raucci, U. D'Amora, A. Ronca, L. Ambrosio, Injectable functional biomaterials for minimally invasive surgery, Adv. Healthc. Mater 9 (13) (2020) 2000349.

[21] Y. Lei, Y. Wang, J. Shen, Z. Cai, C. Zhao, H. Chen, et al., Injectable hydrogel microspheres with self-renewable hydration layers alleviate osteoarthritis, Sci. Adv. 8 (5) (2022) eabl6449, 2022-2-4.

[22] P. Cimavilla-Román, M. Santiago-Calvo, M.Á. Rodríguez-Pérez, Dynamic Mechanical Analysis during polyurethane foaming: relationship between modulus build-up and reaction kinetics, Polym. Test. 103 (2021) 107336.

[23] K. Liu, J. Tong, M. Huang, F. Wang, H. Pang, Model and experimental studies on the effects of load characteristics and polyurethane densities on fatigue damage of rigid polyurethane grouting materials, Constr Build. Mater. 347 (2022) 128595.

[24] M. Li, H. Fang, C. Zhang, M. Du, F. Wang, Study on the new polyurethane material suitable for foaming in water, Construct. Build. Mater. 354 (2022) 129163, 2022-1-1.

[25] J. Liu, J. He, R. Xue, B. Xu, X. Qian, F. Xin, et al., Biodegradation and up-cycling of polyurethanes: progress, challenges, and prospects, Biotechnol. Adv. 48 (2021) 107730.

[26] C.E. Fernández, M. Bermúdez, R.M. Versteegen, E.W. Meijer, G.J. Vancso, S. Muñoz-Guerra, An overview on 12-polyurethane: synthesis, structure and crystallization, Eur. Polym. J. 46 (11) (2010) 2089–2098.

[27] L. Niu, Y. Li, Q. Li, Medicinal properties of organotin compounds and their limitations caused by toxicity, Inorg. Chim. Acta. 423 (2014) 2–13.

[28] T.S. Basu Baul, B. Hlychho, M.R. Addepalli, S. Kundu, D. de Vos, A. Linden, Synthesis and structures of polynuclear organotin(IV) complexes of a polyaromatic carboxylate ligand and cytotoxic evaluation in tumor cell lines, J. Organomet. Chem. 985 (2023) 122592.

[29] T. Laube, J. Weisser, S. Berger, S. Börner, S. Bischoff, H. Schubert, et al., In situ foamable, degradable polyurethane as biomaterial for soft tissue repair, Mater. Sci. Eng. C 78 (2017) 163–174.

[30] H. Wang, J. Zhang, H. Liu, Z. Wang, G. Li, Q. Liu, et al., Chondrocyte-laden gelatin/sodium alginate hydrogel integrating 3D printed PU scaffold for auricular cartilage reconstruction, Int. J. Biol. Macromol. 253 (2023) 126294, 2023-12-31.

[31] M. Chen, Y. Li, S. Liu, Z. Feng, H. Wang, D. Yang, et al., Hierarchical macro-microporous WPU-ECM scaffolds combined with microfracture promote in situ articular cartilage regeneration in rabbits, Bioact. Mater. 6 (7) (2021) 1932–1944, 2021-7-1.

[32] G. Liu, M. Ma, H. Meng, J. Liu, Y. Zheng, J. Peng, et al., In-situ self-assembly of bacterial cellulose/poly(3,4-ethylenedioxythiophene)-sulfonated nanofibers for peripheral nerve repair, Carbohyd Polym. 281 (2022) 119044.

[33] Y. Wang, X. Yu, C. Baker, W.L. Murphy, T.C. McDevitt, Mineral particles modulate osteo-chondrogenic differentiation of embryonic stem cell aggregates, Acta Biomater. 29 (2016) 42–51, 2016-1-1.

[34] X. Zhou, M. Nowicki, H. Cui, W. Zhu, X. Fang, S. Miao, et al., 3D bioprinted graphene oxide-incorporated matrix for promoting chondrogenic differentiation of human bone marrow mesenchymal stem cells, Carbon 116 (2017) 615–624, 2017-5-1.

[35] M. Zhou, N. Lozano, J.K. Wychowaniec, T. Hodgkinson, S.M. Richardson, K. Kostarelos, et al., Graphene oxide: a growth factor delivery carrier to enhance chondrogenic differentiation of human mesenchymal stem cells in 3D hydrogels, Acta Biomater. 96 (2019) 271–280, 2019-9-15.

[36] X. Liu, S. Song, J. Huang, H. Fu, X. Ning, Y. He, et al., HBC-nanofiber hydrogel scaffolds with 3D printed internal microchannels for enhanced cartilage differentiation, J. Mater. Chem. B 8 (28) (2020) 6115–6127.

[37] M. Li, J. Chen, M. Shi, H. Zhang, P.X. Ma, B. Guo, Electroactive anti-oxidant polyurethane elastomers with shape memory property as non-adherent wound dressing to enhance wound healing, Chem. Eng. J. 375 (2019) 121999.

[38] S. Wendels, L. Avérous, Biobased polyurethanes for biomedical applications, Bioact. Mater. 6 (4) (2021) 1083–1106.

[39] C. Zhang, H. Liang, D. Liang, Z. Lin, Q. Chen, P. Feng, et al., Renewable Castor-Oil-based waterborne polyurethane networks: simultaneously showing high strength, self-healing, processability and tunable multishape memory, Angew. Chem. Int. Ed. 60 (8) (2021) 4289–4299, 2021-2-19.

[40] J. Peyrton, L. Avérous, Structure-properties relationships of cellular materials from biobased polyurethane foams, Mater. Sci. Eng. R Rep. 145 (2021) 100608.

[41] J. Reignier, P. Alcouffe, F. Méchin, F. Fenouillot, The morphology of rigid polyurethane foam matrix and its evolution with time during foaming – new insight by cryogenic scanning electron microscopy, J. Colloid Interf Sci. 552 (2019) 153–165.

[42] A. Magnin, E. Pollet, V. Phalip, L. Avérous, Evaluation of biological degradation of polyurethanes, Biotechnol. Adv. 39 (2020) 107457, 2020-1-1.

[43] F. Xie, T. Zhang, P. Bryant, V. Kurusingal, J.M. Colwell, B. Laycock, Degradation and stabilization of polyurethane elastomers, Prog. Polym. Sci. 90 (2019) 211–268.

[44] D. Grzeda, G. Wegrzyk, A. Nowak, J. Idaszek, L. Szczepkowski, J. Ryszkowska, Cytotoxic properties of polyurethane foams for biomedical applications as a function of isocyanate index, Polymers-Basel 15 (12) (2023), 2023-6-20.

[45] F. Zou, H. Meng, M. Ma, F. Han, Y. Wang, Y. Xie, et al., Synergistic strategy constructed novel double-network scaffolds with active micro-environment pH stabilization and M2-macrophage polarization for cartilage defect repair, Compos. B Eng. 258 (2023) 110709, 2023-6-1.

[46] X. Huang, Z. Wang, H. Wang, D. Chen, L. Tong, Novel strategies for the treatment of osteoarthritis based on biomaterials and critical molecular signaling, J. Mater. Sci. Technol. 149 (2023 2023-1-1) 42–55.

[47] X. An, J. Wang, W. Shi, R. Ma, Z. Li, M. Lei, et al., The effect of passive smoking on early clinical outcomes after total knee arthroplasty among female patients, Risk Manag. Healthc. Pol. 14 (2021) 2407–2419.

[48] M.A. Javaid, K.M. Zia, R.A. Khera, S. Jabeen, I. Mumtaz, M.A. Younis, et al., Evaluation of cytotoxicity, hemocompatibility and spectral studies of chitosan assisted polyurethanes prepared with various diisocyanates, Int. J. Biol. Macromol. 129 (2019) 116–126, 2019-1-1.

[49] L. Moradi, M. Vasei, M.M. Dehghan, M. Majidi, S. Farzad Mohajeri, S. Bonakdar, Regeneration of meniscus tissue using adipose mesenchymal stem cells-chondrocytes co-culture on a hybrid scaffold: in vivo study, Biomaterials 126 (2017) 18–30, 2017-1-1.